A Diffusion Model of Binary Systems Controlled by Chemical Potential Gradient

Marek Wróbel[ID], **Andriy Burbelko**[ID]

AGH University of Science and Technology, Faculty of Foundry Engineering, al. A. Mickiewicza 30, 30-059 Krakow
e-mail: marek.wrobel@agh.edu.pl

Abstract

The paper presents a model of diffusion in a single phase with chemical potential gradient as the driving force of the process. Fick's laws are strictly empirical and the assumption that the concentration gradients are the driving forces of diffusion is far from precise. Instead, the gradient of chemical potential μ_i of component i is the real driving force. The matter of governing equations of models that incorporate this approach will be raised and discussed in this article. One of more important features is the ability to acquire results where diffusion against the concentration gradient may occur. The presented model uses the Finite Difference Method (FDM) and employs the CALPHAD method to obtain chemical potentials. The calculations of chemical potential are carried out for instant conditions – temperature and composition – in the entire task domain by Thermo-Calc via a TQ-Interface. Then the heterogeneity of chemical potentials is translated into mass transfer for each individual element. Calculations of two modelling tasks for one-dimension diffusion field were carried out. First: isothermal conditions with linear initial composition distribution and second: constant temperature gradient with uniform chemical composition in the specimen. Results for two binary solid solutions: Fe-C and Fe-Si, in the FCC phase for the given tasks will be presented. Modelling allows us to estimate the time needed to reach a desired state in a particular equilibrium or quasi-equilibrium state. It also shows the path of the composition change during the process. This can be used to determine whether the system at some point is getting close to the formation of another phase due to significant deviation from its initial conditions.

1. INTRODUCTION

Diffusion is one of the phenomena – alongside electrical conduction with Ohm's law, fluid movement with Poiseuille's law, heat flow with Fourier's law – that follows the general relation of transport that is measured by flux [1, 2]:

$$J_x = -L\frac{\partial A}{\partial x} \qquad (1)$$

Although Fick's first law corresponds to Equation (1) it is purely empirical [3, 4] and has limitations in terms of its use. From the fundamental point of view, the assumption that the concentration gradients are the driving forces of diffusion in a multicomponent system is not correct. Instead, the gradient of chemical potential μ_i of component i determines the net flow of that element [5]:

$$J_x = -B_i c_i \frac{\partial \mu_i}{\partial x} \qquad (2)$$

Because determining chemical potential was perhaps not the most convenient way of dealing with the diffusion problem, it was better to express flux entirely in terms of concentration. Since $\mu_i = -\mu_i^0 + RT \ln c_i$, rewriting Equation (2) for uniform temperature gives:

$$J_x = -B_i RT \frac{\partial c_i}{\partial x} \qquad (3)$$

and employing the Nernst–Einstein relation [4]:

$$D_i = B_i RT \qquad (4)$$

gives Fick's first law:

$$J_x = -D_i \frac{\partial c_i}{\partial x} \qquad (5)$$

Analysing the path of the random walk of the particle allows to calculate mean square displacement and with it,

using the Einstein–Smoluchowski Equation [6] – diffusion coefficient [7]:

$$\langle x^2 \rangle = 2Dt \qquad (6)$$

Fick's first law, however, applies to diffusion events where the rate of transport is steady state; that is the rate of flux is constant [8]. For that reason, the phenomenological relation given by Equation (2) was used in the model.

2. FDM MASS TRANSPORT EQUATIONS

Below is the derivation of general formula for mass transport for three-dimension calculations. Its special case for one-dimension is incorporated into the model presented in this paper.

According to the divergence theorem [9], for any closed space with volume V and external surface S total mass of an element m_i can be calculated by integration over volume of this body:

$$m_i = \iiint\limits_V m_i \, dx \, dy \, dz \qquad (7)$$

and the rate of change of that mass by integrating over its surface:

$$\frac{\partial m_i}{\partial \tau} = \iint\limits_S \mathbf{J}_i \cdot d\mathbf{s} \qquad (8)$$

where the operator " $\cdot$ " stands for scalar product. Inputting Equation (2) we get:

$$\frac{\partial m_i}{\partial \tau} = -\iint\limits_S B_i c_i \nabla \mu_i \cdot d\mathbf{s} \qquad (9)$$

Numerical approximation of Equation (9) can be obtained by replacing differentials with finite differences. In differential calculations, using control volumes method, for finite cuboidal control volume with dimensions Δx, Δy and Δz, this equation converts to (element's index has been dropped):

$$
\begin{aligned}
\frac{\Delta m_0}{\Delta \tau} = & -B_{x+} \frac{c_{x+} + c_0}{2} \frac{\mu_{x+} - \mu_0}{\Delta x} \Delta y \Delta z + \\
& -B_{x-} \frac{c_{x-} + c_0}{2} \frac{\mu_{x-} - \mu_0}{\Delta x} \Delta y \Delta z + \\
& -B_{y+} \frac{c_{y+} + c_0}{2} \frac{\mu_{y+} - \mu_0}{\Delta y} \Delta x \Delta z + \\
& -B_{y-} \frac{c_{y-} + c_0}{2} \frac{\mu_{y-} - \mu_0}{\Delta y} \Delta x \Delta z + \\
& -B_{z+} \frac{c_{z+} + c_0}{2} \frac{\mu_{z+} - \mu_0}{\Delta z} \Delta x \Delta y + \\
& -B_{z-} \frac{c_{z-} + c_0}{2} \frac{\mu_{z-} - \mu_0}{\Delta z} \Delta x \Delta y
\end{aligned}
\qquad (10)
$$

where index 0 refers to values of concentration, chemical potential or mobility for the considered cell whereas indexes x, y, z along with signs ± determines values of those quantities for neighbouring cells along given axis and in specified direction. Figure 1 presents the mutual location of the origin cell and its neighbours.
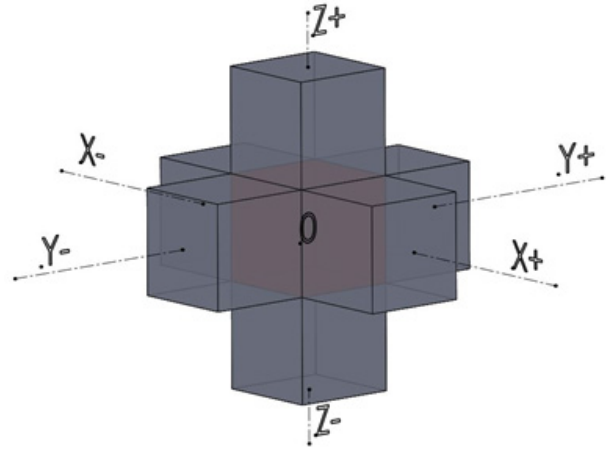
Fig. 1. Mutual location of origin cell 0 and its neighbouring cells $x\pm$, $y\pm$, $z\pm$

For cubic grid with edge Δx Equation (10) can be simplified as:

$$
\begin{aligned}
\frac{\Delta m_0}{\Delta \tau} = & -B_{x+} \frac{c_{x+} + c_0}{2} \left(\mu_{x+} - \mu_0 \right) \Delta x + \\
& -B_{x-} \frac{c_{x-} + c_0}{2} \left(\mu_{x-} - \mu_0 \right) \Delta x + \\
& -B_{y+} \frac{c_{y+} + c_0}{2} \left(\mu_{y+} - \mu_0 \right) \Delta x + \\
& -B_{y-} \frac{c_{y-} + c_0}{2} \left(\mu_{y-} - \mu_0 \right) \Delta x + \\
& -B_{z+} \frac{c_{z+} + c_0}{2} \left(\mu_{z+} - \mu_0 \right) \Delta x + \\
& -B_{z-} \frac{c_{z-} + c_0}{2} \left(\mu_{z-} - \mu_0 \right) \Delta x
\end{aligned}
\qquad (11)
$$

With the assumption that mobility B is constant, after rearranging we get:

$$
\begin{aligned}
\Delta m_0 = & \frac{-B \Delta x \Delta \tau}{2} \times \\
& \times [\left(c_{x+} + c_0 \right)\left(\mu_{x+} - \mu_0 \right) + \left(c_{x-} + c_0 \right)\left(\mu_{x-} - \mu_0 \right) + \\
& + \left(c_{y+} + c_0 \right)\left(\mu_{y+} - \mu_0 \right) + \left(c_{y-} + c_0 \right)\left(\mu_{y-} - \mu_0 \right) + \\
& + \left(c_{z+} + c_0 \right)\left(\mu_{z+} - \mu_0 \right) + \left(c_{z-} + c_0 \right)\left(\mu_{z-} - \mu_0 \right)]
\end{aligned}
\qquad (12)
$$

By shortening the expression we get the following form of the difference equation for the change of mass of an element in time:

$$\Delta m_0 = \frac{-B \Delta x \Delta \tau}{2} \sum_{dir=1}^{p} \left[\left(c_{dir} + c_0 \right)\left(\mu_{dir} - \mu_0 \right) \right] \qquad (13)$$

In the presented model we track the mass of each element in every cell therefore concentration c is a known value. Mobility B is assumed to be constant for each element. It was calculated using Equation (4) using diffusion coefficients given later. Δx and $\Delta \tau$ are respectively space and time grid steps. The problem of employing Equation (13) rests on the ability to determine the values of chemical potential for each element for the given conditions – composition and temperature.

3. CALPHAD CALCULATIONS

The CALPHAD method, taking its name from CALculations of PHAse Diagrams, gives way to determining the state of a system by the means of calculating it. In other words, it is computational thermodynamics, as in the title of reference [10]. The method allows, among the others, to calculate which phases will be stable and what composition they will have in the equilibrium state, what will be values of thermodynamic quantities for a system or a phase. One of the values that can be calculated in this way is chemical potential, in this case using Thermo-Calc Software – a program basing on CALPHAD method. Detailed information about the topic can be found in [10–13].

Since the presented model needs up-to-date values of μ_i, for every calculation timestep, it is not possible to make one-time calculations using Thermo-Calc and incorporate the result into the model's algorithm. There is a need for the constant exchange of data between routines using Equation (13) in the model and the Thermo-Calc program: new, updated masses of elements in the cell are sent – new values of chemical potentials are being received. Thermo-Calc offers three Software Development Kits that allows such communication, with the TQ-Interface used in the present work. A broad description of acquiring data needed by modelling module can be found in a previous work by the authors [14].

Calculations of the chemical potentials used by the model were made using a Thermo-Calc 2019a with TQInterface and thermodynamic database TCFE7.

4. CALCULATION DESCRIPTION

A simulation of one-dimension diffusion field for two binary systems: Fe-C and Fe-Si, was carried out. For each system, two separate calculation tasks were performed:

1) isothermal conditions with linear composition distribution,
2) constant temperature gradient with uniform chemical composition in the specimen.

Due to the significant difference in the values of mobility of carbon and silicon, the total modelled length of the specimen was chosen individually for each system. In both cases the number of grid cells was equal to 100. Temperature and concentration were chosen to put the system within the range of single (FCC) phase in phase diagrams.

Diffusion coefficients, used to determine values of mobility, were calculated with the use of the Arrhenius Equation:

$$D = D_0 \exp\left(\frac{-Q}{RT}\right) \qquad (14)$$

The following values of D_0 and Q were used:

- for D_{Fe}: $D_0 = 4.085$ cm$^2 \cdot$ s^{-1}, $Q = 311.1$ kJ $\cdot$ mol^{-1}[15],
- for D_C: $D_0 = 0.234$ cm$^2 \cdot$ s^{-1}, $Q = 147.81$ kJ $\cdot$ mol^{-1} [15],
- for D_{Si}: $D_0 = 0.07$ cm$^2 \cdot$ s^{-1}, $Q = 243.0$ kJ $\cdot$ mol^{-1} [16].

For each system temperature of task (1) was used in the Equation (14), which is also mean temperature of task (2).

4.1. Fe-C system

Table 1 contains values of the parameters used in the calculations. A total length of 50 mm was modelled.

Table 1
Data used for simulation of Fe-C system

Quantity	Value	Unit
Δx	5E-4	[m]
D_{Fe}	7.04156E-17	[m$^2 \cdot$ s^{-1}]
D_C	2.01838E-11	[m$^2 \cdot$ s^{-1}]
For task (1)		
T	1000	[°C]
$c_{C, min}$	0.5	[wt.%]
$c_{C, max}$	1.0	[wt.%]
For task (2)		
$T_{min (x = 0 mm)}$	950	[°C]
$T_{max (x = 50 mm)}$	1050	[°C]
c_C	0.75	[wt.%]

Figures 2–4 present the results of the simulation for task (1). The composition curves, for $\tau > 0$, in Figure 2 are not symmetrical with respect to the point in the middle of the plot (25 mm, 0.75 wt.% C). The curves close to $\tau = 0$, e.g. curve **b** do not overlap line **a**. Though small, there is non-zero difference of carbon concentration between **a** and **b** across whole distance.
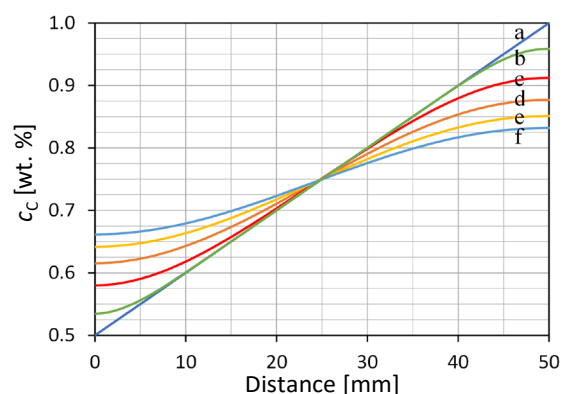

Fig. 2. Initial concentration of carbon (a) and modelled distribution after: b) 5 days; c) 25 days; d) 50 days; e) 75 days; f) 100 days; Fe-C, task (1)
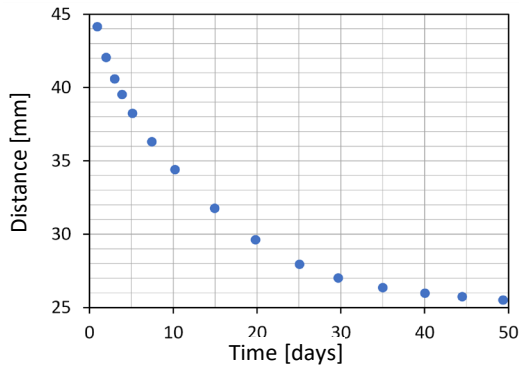
Fig. 3. Position of point with equal to initial concentration of carbon; Fe-C, task (1)
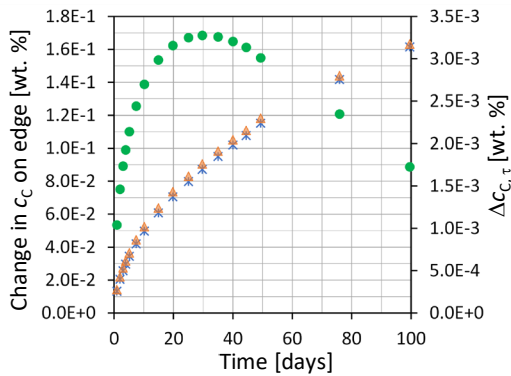

Fig. 4. Change of c_C with respect to initial values for $x = 0$ (star), $x = 50$ mm (triangle) and difference of those two (circle); Fe-C, task (1)

Because on one edge c_C with time increases and on the other – decreases the point, where **a** crosses any composition curve for $\tau > 0$, can be distinguished. Figure 3 shows the position of this point of cross where the calculated concentration of carbon is equal to the initial. In early stages it is close to the end with $c_C = 1.0$ wt.% and in time it asymptotically tends to the middle of the specimen. Figure 4 shows changes in carbon concentration on both edges, at $x = 0$, $x = 50$ mm as well as varying difference of those two, defined for element i as:

$$\Delta c_{i,\tau=t_1} = \left| c_{i,\tau=t_0,x=50} - c_{i,\tau=t_1,x=50} \right| + \\ - \left| c_{i,\tau=t_1,x=0} - c_{i,\tau=t_0,x=0} \right| \tag{15}$$

The difference has its maximum at $\tau \approx 30$ days and then slowly decreases as the system tends to equilibrium, where $\Delta c_{C,\tau=\infty} = 0$.

Figures 5–7 present the results for the modelling of task (2). Similarly to task (1), the curves in Figure 5 for $\tau > 0$ are not symmetrical with respect to the point in the middle of the plot (25 mm, 0.75 wt.% C). It is noteworthy that task (2) presents a situation where diffusion occurs with initially zero and shortly even against concentration gradient. A similar uphill diffusion was observed by Darken in [17] for a higher order system. Figure 6 shows the position of a point with equal to initial concentration of carbon. In the early stages it is close to the end with $T = 1050°C$ ($x = 50$ mm) and in time it asymptotically tends to the point close to the middle of the specimen. In case of task (2) however there

is no certainty of final location of that point nor values of $c_{C,x=0}$ and $c_{C,x=50}$ for $\tau = \infty$ as they depend on chosen temperature. Figure 7 confirms that carbon concentrations do not tend to a straight line symmetrical with respect to the middle point as the difference in carbon gain at $x = 50$ mm and carbon loss at $x = 0$ cells, within calculated 100 days, constantly increases.
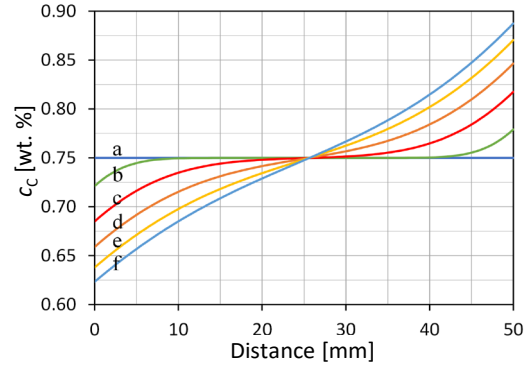

Fig. 5. Initial concentration of carbon (a) and modelled distribution after: b) 5 days; c) 25 days; d) 50 days; e) 75 days; f) 100 days; Fe-C, task (2)
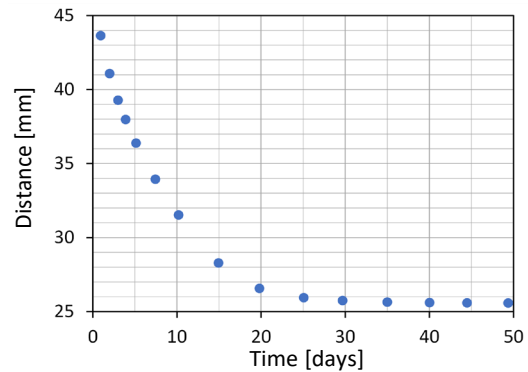

Fig. 6. Position of point with equal to initial concentrations of carbon; Fe-C, task (2)
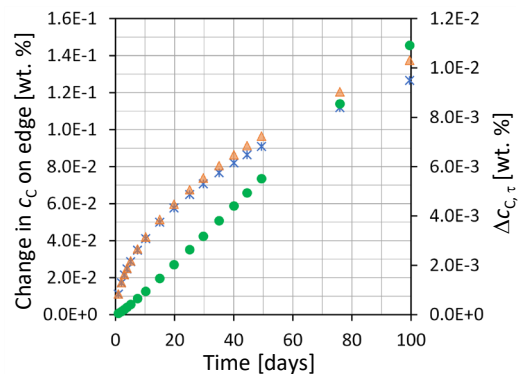

Fig. 7. Change of c_C with respect to initial values for $x = 0$ (star), $x = 50$ mm (triangle) and difference of those two (circle); Fe-C, task (2)

4.2. Fe-Si system

Table 2 contains values of parameters used in calculations. A total length of 1 mm was modelled. The results are analogical to the Fe-C system.

Table 2
Data used for simulation of Fe-Si system

Quantity	Value	Unit
Δx	1E-5	[m]
D_{Fe}	3.80618E-15	[m$^2 \cdot$ s^{-1}]
D_{Si}	1.69443E-14	[m$^2 \cdot$ s^{-1}]
For task (1)		
T	1200	[°C]
$c_{Si\ min}$	0.05	[wt.%]
$c_{Si,\ max}$	1.55	[wt.%]
For task (2)		
$T_{min\ (x = 0\ mm)}$	1150	[°C]
$T_{max\ (x = 50\ mm)}$	1250	[°C]
c_{Si}	0.80	[wt.%]

Fig. 9. Position of point with equal to initial concentrations of silicon; Fe-Si, task (1)

Fig. 10. Change of c_{Si} with respect to initial values for $x = 0$ (star), $x = 1$ mm (triangle) and difference of those two (circle); Fe-Si, task (1)

Figures 8–10 present results of simulation for task (1). Composition curves, for $\tau > 0$, in Figure 8 are not symmetrical with respect to the point in the middle of the plot (0.5 mm, 0.80 wt.% Si). Figure 9 shows the position of the point with equal to initial concentrations of silicon. In the early stages it is close to the end with c_{Si} = 1.55 wt.% and in time it asymptotically tends to the middle of the specimen. Figure 10 shows varying differences in silicon loss at $x = 1.0$ mm and silicon gain at $x = 0$ cells calculated using Equation (15).

It has a maximum at $\tau \approx 15$ days and then slowly decreases as the system tends to equilibrium, where $\Delta c_{Si,\ \tau = \infty} = 0$.

Difference in silicon loss at $x = 50$ mm and silicon gain at $x = 0$ cells; Fe-Si, task (1).
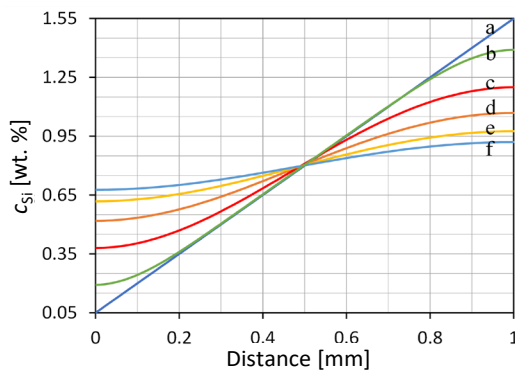
Figures 11–13 present results for modelling of task (2). Similarly to task (1), the curves in Figure 11 for $\tau > 0$ are not symmetrical with respect to the point in the middle of the plot (0.5 mm, 0.80 wt.% Si). Again, it is situation where uphill diffusion occurs. Figure 12 shows position of point with equal to initial concentrations of silicon. In the early stages it is close to the end with $T = 1250$°C ($x = 1.0$ mm) and in time it asymptotically tends to the point close to the middle of the specimen. Figure 13 confirms that silicon concentration do not tend to a straight line symmetrical with respect to the middle point as the difference in silicon gain at $x = 50$ mm and carbon loss at $x = 0$ cells, within calculated 100 days, constantly increases.

Fig. 8. Initial concentration of silicon (a) and modelled distribution after: b) 5 days; c) 25 days; d) 50 days; e) 75 days; f) 100 days; Fe-Si, task (1)
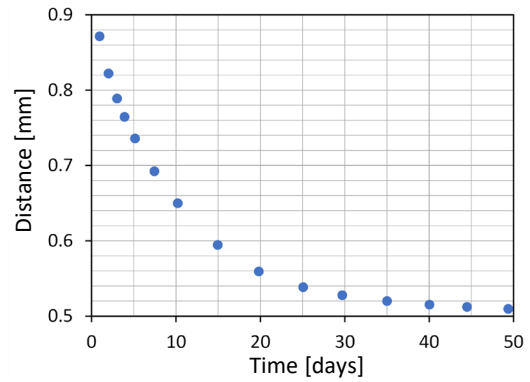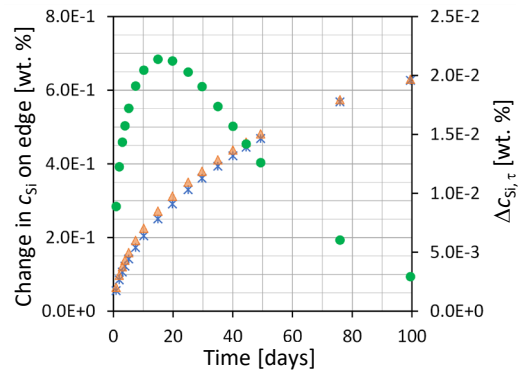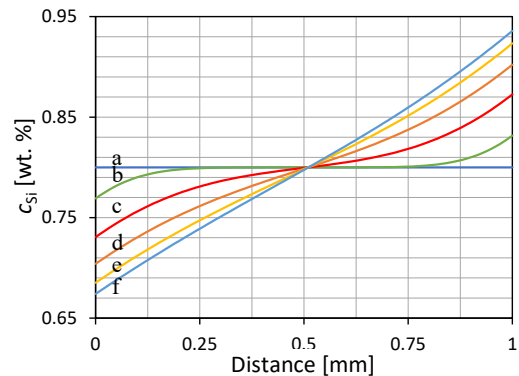

Fig. 11. Initial concentration of silicon (a) and modelled distribution after: b) 5 days; c) 25 days; d) 50 days; e) 75 days; f) 100 days; Fe-Si, task (2)
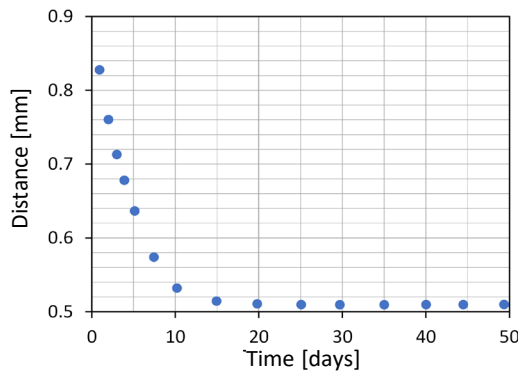
Fig. 12. Position of point with equal to initial concentration of silicon; Fe-Si, task (2)
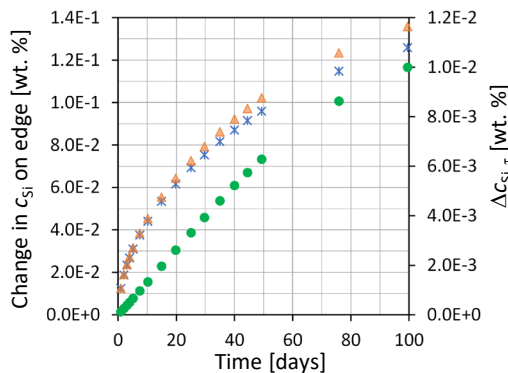

Fig. 13. Change of c_{Si} with respect to initial values for $x = 0$ (star), $x = 1$ mm (triangle) and difference of those two (circle); Fe-Si, task (2)

5. CONCLUSIONS

The conditions in which the presented model can be utilised, together with its major features, are summarised below:

- For task (1), the difference in chemical composition in a uniform temperature field leads to the occurrence of chemical potential gradient and non-zero values of fluxes of elements in the system.
- For task (2), the chemical potential gradient is present, despite the initial equality of chemical composition, because of the dependency of chemical potentials on temperature.
- The model uses a single set of equations to determine fluxes for both sources of the difference in chemical potentials.
- For task (2), uphill diffusion (against chemical composition gradient) has been observed, which is not achievable with a model based on Fick's laws.

The model can be used to evaluate the kinetics of changes to a concentration profile for a specimen exposed to non-uniform temperature field which give a view on the time needed to reach a pre-assumed state of interest.

REFERENCES

[1]   Bergethon P.R. & Simons E.R. (1990). *Biophysical Chemistry: Molecules to Membranes*. New York: Springer-Verlag.
[2]   Shewmon P. (2016). *Diffusion in Solids*. Cham: Springer International Publishers.
[3]   Bhadeshia H.K.D.H. (2021). *Course MP6: Kinetics & Microstructure Modelling. University of Cambridge*. Retrieved from: https://www.phase-trans.msm.cam.ac.uk/teaching.html [23.08.2021].
[4]   Mehrer H. (2007). *Diffusion in Solids: Fundamentals, Methods, Materials, Diffusion-Controled Processes*. Berlin – Heidelberg: Springer-Verlag.
[5]   Porter D.A., Easterling K.E. & Sherif M.Y. (2009). *Phase Transformations in Metals and Alloys*. Boca Raton: CRC Press.
[6]   Tilley R.J.D. (2004). *Understanding Solids: The Science of Materials*. Chichester: John Wiley & Sons.
[7]   Ernst D. & Kohler J. (2013). Measuring a diffusion coefficient by single-particle tracking: statistical analysis of experimental mean squared displacement curves. *Physical Chemistry Chemical Physics*, 15(3), 845–849. Doi: https://doi.org/10.1039/c2cp43433d.
[8]   Bergethon P.R. (2000). *The Physical Basis of Biochemistry*. New York: Springer Science + Business Media.
[9]   Spiegel M.R. (1959). *Vector Analysis*. New York: McGraw-Hill.
[10] Lukas H.L., Fries S.G. & Sundman B. (2007). *Computational Thermodynamics*. Cambridge: Cambridge University Press.
[11] Zabdyr L. A. (2005). *Strategia CALPHAD*. Kraków: Instytut Metalurgii i Inżynierii Materiałowej PAN.
[12] Spencer P.J. (2008) A brief history of CALPHAD. *Calphad*, 32(1), 1–8. Doi: https://doi.org/10.1016/j.calphad.2007.10.001.
[13] Wróbel M. & Burbelko A. (2013). Wykorzystanie programów komputerowych do obliczeń termodynamicznych w procesach metalurgicznych: metoda CALPHAD. In: Holtzer M., P*rocesy metalurgiczne i odlewnicze stopów żelaza: podstawy fizykochemiczne*. Warszawa: Wydawnictwo Naukowe PWN, 512–534.
[14] Wróbel M. & Burbelko A. (2014). Retrieval of Thermodynamic Data for Modelling of Solidification Using TQ Interface. *METAL 2014: 23rd International Conference on Metallurgy and Materials,* May 21–23 Brno. (pp. 99-104). Ostrava: Tanger.
[15] Brandes E.A. & Brook G.B. (Eds.) (1998). *Smithells Metals Reference Book*. 7th Edition. Oxford: Elsevier.
[16] Bergner D., Khaddour Y. & Lorx S. (1989). Diffusion of Si in bcc- and fcc-Fe. *Defect and Diffusion Forum*, 66–69, 1407–1412. Doi: https://doi.org/10.4028/www.scientific.net/DDF.66-69.1407.
[17] Darken L.S. (1949). Diffusion of Carbon in Austenite with a Discontinuity in Composition. *Transactions of the AIME*, 180, 430–438.

LIST OF VARIABLES USED IN THE TEXT

$\partial A/\partial x$ – gradient of potential in general flux equation

μ_i – chemical potential of element i

τ – time variable

B_i – mobility of element i

c_i – composition of element i

D_0 – coefficient in Arrhenius Equation

D_i – diffusion coefficient of element i

dir – direction in which neighbouring cell is located: $x\pm$, $y\pm$, $z\pm$

J_x – flux in x direction

L – coefficient in general flux equation

m_i – mass of element i

p – number of directions taking into account in calculations: for model 1D: $p = 2$, 2D: $p = 4$, 3D: $p = 6$

Q – activation energy in Arrhenius Equation

R – gas constant

T – absolute temperature

t – time

x, y, z – space variables